Green Chemistry

PAPER

View Article Online
View Journal | View Issue

Cite this: *Green Chem.*, 2021, **23**, 3740

Catalytic hydrogenation of CO_2 from air *via* porous silica-supported Au nanoparticles in aqueous solution†

Siting Ni, [a] Jun Zhu, [a] Ranjan Roy,[b] Chao-Jun Li [a] and R. Bruce Lennox*[a]

Received 19th December 2020,
Accepted 21st April 2021

DOI: 10.1039/d0gc04303f

rsc.li/greenchem

The conversion of the ubiquitous greenhouse gas CO_2 to valuable organic products is much sought after. Herein, the hydrogenation of CO_2 to C1 products with an 80% yield in water is reported using a novel catalyst, porous-silica-supported Au nanoparticles (Au/SiO_2). In the presence of a Lewis acid, boric acid, the Au/SiO_2 catalyst enables an efficient conversion of amine-captured CO_2 to methanol, formate, and formamide. A mechanistic study involving isotopic labelling suggests that methanol production in the catalytic process arises from the direct hydrogenation of formate. Most importantly, this one-pot, two-step process is able to convert CO_2 in air at ambient pressures to C1 products in the absence of an organic solvent. Furthermore, the catalyst is readily recycled without further purification or reactivation and shows no significant decrease in catalytic activity after four reaction cycles in a reusability test.

Introduction

Given the increasing levels of CO_2 in the atmosphere[1] and the increasing use of fossil fuels around the World, it is recognized that the capture, utilization, and storage of CO_2 is necessary.[2] Formic acid and methanol are two common, and versatile, products of the hydrogenation of CO_2. Formic acid is widely used in food preservation, leather and rubber production, cleaning supplies manufacture, fuel cells, and hydrogen storage.[3] Methanol not only serves as a fundamental reagent in chemical production but also used as a fuel in fuel cells.[4] Extensive efforts have been reported in the development of catalysts for the hydrogenation of CO_2 to produce methanol and formic acid.[5] The CO_2 sources for hydrogenation include combustion processes (pre-, during, or post-) or ambient air. The latter, known as direct air capture (DAC), has either location limitations or contamination removal challenges in flue gas capture.[6] Recently, DAC has been incorporated in tandem processes, where CO_2 is efficiently converted to methanol and formic acid, despite being a dilute CO_2 source.[7]

Approaches to the catalytic hydrogenation of CO_2 include photochemical, electrochemical, and thermal chemical reductions.[5,8] Compared to homogenous catalysis, heterogeneous CO_2 reduction in water is particularly sought-after for two reasons. Firstly, heterogeneous catalysts can often be relatively easily recovered from the reaction mixture.[9] Moreover, the accelerated cleaning process usually avoids the usage of organic solvents, whereas the use of organic solvents is common in homogenous catalyst extraction/cleaning processes. Secondly, water is an attractive solvent in scale-up[10] and can often be viewed as a green solvent.[11]

A basic environment, usually involving the addition of amines or buffers, facilitates CO_2 capture and enhances conversion efficiency. The actual starting materials in base-assisted CO_2 hydrogenation are usually (bi)carbonates and carbamates, serving to significantly lower the energy barrier of C=O conversion.[12] Aqueous amine solutions can also be used to capture/separate CO_2 from both air and various gas mixtures *via* amine scrubbing.[13] The resulting CO_2 capture solution can be a convenient way to store CO_2. It can be used directly, and is widely used in industry as such for further use.[14]

Heterogeneous catalysts, especially supported nanoparticles, have been demonstrated in several reports to have excellent catalytic properties in CO_2 hydrogenation in a basic aqueous environment. Several recent examples included PdAu on graphene oxides with amine moieties,[15] PdAg on mesoporous carbon with modified amines,[16] PdAg on TiO_2,[17] Co on nitrogen-rich graphitic carbon,[18] and nanoporous nickel.[3] Each of these examples uses additives (KOH, $NaHCO_3$, amine) to render the overall aqueous environment basic, or directly use (bi)carbonates as the starting materials. The principal

[a]*Department of Chemistry, McGill University, 801 Sherbrooke St West, Montreal, Quebec H3A 0B8, Canada. E-mail: bruce.lennox@mcgill.ca*
[b]*Department of Chemical Engineering, McGill University, M.H. Wong Building, Montreal, Quebec H3A 0C5, Canada*

†Electronic supplementary information (ESI) available. See DOI: 10.1039/d0gc04303f

product of the resulting hydrogenations is formate, while the secondary products depend on the specific catalyst used.

In addition to the above-mentioned metallic nanoparticles, metal oxide-supported Au nanoparticles have emerged as versatile heterogeneous catalysts in CO_2 hydrogenation. Early work on the Au-catalyzed CO_2 hydrogenation to C1 products did not usually involve liquid phases, exhibited a high CO content in the products and low catalyst recyclability, and involved relatively harsh reaction conditions.[19,20] This type of solid–gas process was later improved upon,[21] but is still difficult to incorporate with DAC. For Au-catalyzed CO_2 hydrogenation to C1 products involving solvents or liquids, Au nanoparticles supported by oxides (such as TiO_2, Al_2O_3, CeO_2, ZrO_2, SiO_2) catalytically convert CO_2 principally to formate/formic acid, either in a polar organic environment or in a neat state with addition of organic amines.[22–24] Nevertheless, some of these liquid-phase-involved systems require the use of organic solvents, otherwise they demonstrate low turnover number (TON).[23] Other reactions are either base-free[24] or require pure gases at high pressure as starting material.[22] These are thus very unlikely to be directly re-purposed for DAC or DAC-incorporated tandem conversions. Liu and co-workers[25] recently reported an Au nanocluster catalyst supported on Schiff-base-modified SiO_2 substrates. This system was able to catalytically hydrogenate CO_2 in a neat or partially aqueous environment with the assistance of NEt_3 under moderate pressure (80 bar) and moderate temperature (90 °C). However, the high catalytic activities were compromised by the rapid aggregation of Au nanoclusters, resulting in a ~50% drop in TON after three cycles. These results indicate that approaches to heterogeneous Au(0) catalysis can be fruitful in amine-assisted CO_2 hydrogenation in water. This is especially the case in addressing the need for DAC-incorporated tandem conversion, catalyst stability, and reusability.

The structure of the support nanostructure is essential in the design of an efficient Au(0) catalyst for use in mild, aqueous conditions. Mesoporous silica is an interesting candidate for a support as it provides controllable porosity structures, enabling extensive dispersion of the nanoparticle catalyst, while maintaining access of the reactants to the active metal sites.[26–28] Mesoporous silica can also affect the selectivity of a given reaction due to pore size effects and the interaction with metal nanoparticles, controlled by the specific structure of the particular silica used.[29]

With these considerations in mind, we have developed a two-step amine-assisted CO_2 hydrogenation system which uses porous-silica-supported Au nanoparticles (Au/SiO_2) as the catalyst (Scheme 1). The Au/SiO_2 has mesoporous silica beads whose nanostructures result from micellar templates, where 4-dimethylaminopyridine (DMAP)-capped AuNPs are embedded in the pores of micron-scale SiO_2 beads. Compared to other methods to prepare supported metal nanoparticles for catalytic purposes, the approach used here ensures the control of the AuNP sizes and morphologies.[30] The Au/SiO_2 reported here has a well-defined nanostructure with a high Au(0) loading (5.55 wt%). The Au/SiO_2 can be used at least four times without losing significant catalytic activity. Furthermore, the recycled catalyst does not require a special activation process, enabling a one-pot separation-free system when (re)using the catalyst. The "capture-hydrogenation" two-step strategy significantly expands the range of usable CO_2 sources, including the direct use of ambient air. CO_2 hydrogenation reactions was carried out at 16 bar and 100 °C in water, and no ultrahigh-pressure equipment is required. 80% of CO_2 was converted within 48 hours to yield three C1 products: formate, formamide, and methanol. A mechanistic study suggests that the methanol under these conditions originates from the direct hydrogenation of formate. The system featuring this novel Au/SiO_2 catalyst demonstrates promise in the scale up of CO_2 conversion from air given its advantages in the absence of organic solvent usage, facile catalyst reuse, and high conversion efficiency under relatively mild (hydrogenation) conditions.

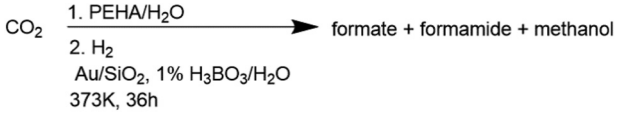

Scheme 1 The general reaction scheme.

Experimental

Materials

Hexadecyltrimethylammonium bromide (commonly known as cetyltrimethylammonium bromide, CTAB, ≥99%), tetramethyl orthosilicate (TMOS, 98%), 1,3,5-trimethylbenzene (TMB, 98%), pentaethylenehexamine (PEHA, technical grade), and water–^{18}O (97 atom% ^{18}O) were purchased from Sigma-Aldrich. Methanol (ACS certified), anhydrous ethanol (ACS certified), and sodium hydroxide (Pellet, ACS certified) were purchased from Fisher Scientific. Water used in preparation procedures was obtained from a Milli-Q system (18 MΩ) except otherwise indicated. All additional chemicals were obtained from commercial suppliers and were used without further purification.

Preparation of the catalyst: porous-silica-supported Au nanoparticles (Au/SiO_2)

Silica beads with high porosity were prepared *via* a modified Stöber method,[31] followed by a pore expansion process using the "swelling agent incorporation method" (Scheme 2).[32] The modified Stöber method yields porous silica beads (d = 500 nm) with nanoscale size pores. The pore expansion process enlarges those pores to approximately 20 nm in diameter. This resulting pore structure allows 5 nm AuNPs to be tightly retained. The resulting porous silica beads embedded with AuNPs are designated as Au/SiO_2 in the following text.

Characterizations of Au/SiO_2

The weight percent (5.55 ± 0.06%) of Au in Au/SiO_2 was determined by inductively coupled plasma optical emission spec-

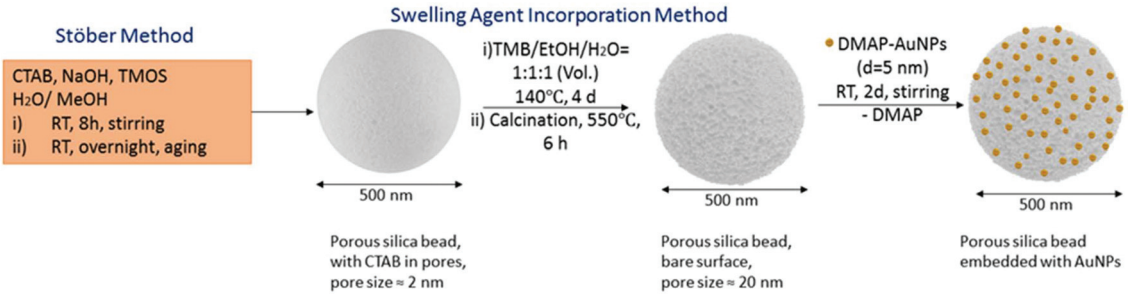

Scheme 2 Preparation of Au/SiO_2 catalysts.

trometry (ICP-OES). The loading efficiency was similar to that of other previously reported Au–SiO_2 composites,[33] but greater than ones prepared for catalytic purposes (*ca.* 1–2%).[34] Zeta potential measurements (ESI, Table S1†) indicate that the underivatized porous silica beads are negatively charged, whereas DMAP-AuNPs are positively charged. After the AuNPs are embedded in the pores, the zeta potential of the Au/SiO_2 is slightly more positive than the SiO_2 alone.

The morphologies of the silica beads before and after being infiltrated by AuNPs were examined by TEM (Fig. 1A–D) and SEM (Fig. 1E and F). Both TEM and SEM images show that the porous silica beads (d = 500 nm) have extensive porosity and that the porous channels are not restricted to the surface region of the bead and in fact reach the center of the beads. Both TEM and SEM images show the presence of AuNPs inside the porous silica beads after exposure to AuNPs. The presence of Au in the Au/SiO_2 composites was further confirmed by elemental analysis. Both EDS (Fig. S1†) and XPS (Fig. 2A) confirm the presence of Au in the silica beads. The binding energy scan in the XPS N 1s region (Fig. 2B) shows the loss of the DMAP-derived N peak in the Au/SiO_2 composites. The XPS binding energy scan in the Au 4f region (Fig. 2C) demonstrates the interaction between the gold and SiO_2, where peaks at 83.80 eV ($Au\ 4f_{7/2}$) and 87.55 eV ($Au\ 4f_{5/2}$) for the Au/SiO_2 composite are observed, compared to 84.16 eV and 87.87 eV for the precursor DMAP-coated AuNPs. This binding energy shift is consistent with a charge transfer process arising between the SiO_2 and AuNP.[35] Moreover, compared to free AuNP, the silica-associated AuNPs exhibit broadened Au 4f peaks, as per the broadened peaks observed in aggregated AuNPs.[36]

In terms of catalyst function, the porous silica provides both a solid support for the AuNPs as well as a means to prevent the AuNPs from aggregating during the course of the CO_2 reaction. A stability test (Fig. S5†) shows that the Au/SiO_2 composites are able to withstand prolonged sonication. A BET (Brunauer–Emmett–Teller) analysis determined that the Au/SiO_2 composites have a surface area of 202.65 $m^2\ g^{-1}$ with an average adsorption pore width of 6.94 nm, whereas the original porous SiO_2 support has a surface area of 268.6 $m^2\ g^{-1}$ with an adsorption average pore width of 6.99 nm. This surface area is similar to that reported for Au-containing metal oxide porous materials.[37] The small difference in BET-derived average pore widths is consistent with the AuNPs being embedded inside

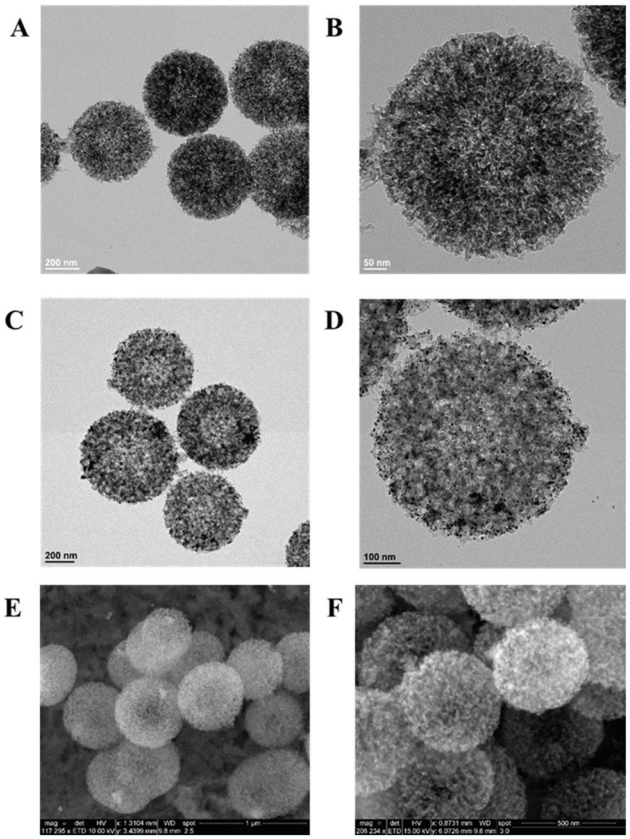

Fig. 1 Morphologies of porous SiO_2 and Au/SiO_2. Rows one and two: TEM images of porous silica beads (A and B) before and (C and D) after the AuNPs embedding. The dark spots presented in (C and D) are AuNPs. Row three: SEM images of porous silica beads (E) before and (F) after the AuNPs embedding. The bright spots presented in (F) are AuNPs.

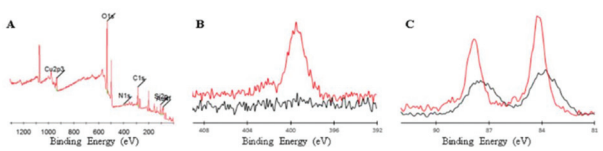

Fig. 2 XPS characterization of Au/SiO_2 and AuNP. (A) XPS survey scan of porous silica beads embedded with AuNPs. XPS binding energy in (B) N 1s region, between DMAP-AuNPs (red) and porous silica beads embedded with AuNPs (black); (C) Au 4f region, between DMAP-AuNPs (red) and porous silica beads embedded with AuNPs (black).

the silica pores rather than blocking access to the pores. Pore-blocking usually results in a significant decrease in both BET-derived surface area values as well as pore volume values.[38]

Experimental procedure

In a typical CO_2 capture process, 0.1 g PEHA (pentaethylenehexamine) was dissolved in 3 mL water, forming a 3.2 wt% PEHA solution. In a pressure tube reactor, an excess quantity (*cf.* amine) of CO_2 was introduced into the solution and maintained at 70 °C for 4 hours. In the case where the CO_2 was directly captured from air, air was continuously bubbled into 30 mL of the 3.2 wt% PEHA solution for 48 hours at room temperature, with stirring. A known quantity of internal standard (imidazole) was added to a portion of the resulting CO_2 capture solution, followed by quantitative ^{13}C NMR measurements (details in ESI†) to identify products and their respective quantities.

In a typical CO_2 hydrogenation reaction, 600 μL of the CO_2 capture solution, 5.29 mg Au/SiO_2 suspended in 992 μL water, and 8.62 μL 0.1 M boric acid aqueous solution (1 mol% boric acid) were mixed into a pressure tube reactor. After purging with H_2, the tube was charged with 16 bar H_2 (25 °C). The entire system was then stirred at 100 °C for 48 hours. The system was manually vented after cooling to room temperature. The gas phase was collected, showing no detectable gaseous product by GC-TCD (details in ESI†). After removing the catalyst by centrifugation, a known quantity of the internal standard (imidazole) and an appropriate quantity of D_2O were added to the liquid phase, the resulting mixture was examined to identify products and their respective yields.

Results and discussion

Effect of PEHA wt% on the captured species and the hydrogenated products

After the aqueous amine solutions were purged with CO_2, a mixture of bicarbonates and carbamates is produced. In the case of PEHA, the ratio of bicarbonates to carbamates, and the total CO_2 capacity principally depend on the wt% of PEHA in water.[39] To determine if the CO_2 capacity (the extent of PEHA reacted with CO_2) influences the yield in the hydrogenation reaction and if the hydrogenation of bicarbonates and carbamates proceeds at different rates or mechanisms (further explored in section Mechanistic studies), we investigated the influence of the PEHA wt% on the captured species and the resulting hydrogenated products.

A series of PEHA solutions involving a range of wt% values was prepared. The CO_2 capture method depends on the wt% of PEHA solutions. For example, 3 mL of the low wt% PEHA solutions (3.2 wt%, 11 wt%, and 20 wt%) was exposed to an excess quantity of CO_2 (3 bar, 10 bar, or 10 bar, respectively) at 70 °C for 4 hours with stirring. For the case of the high wt% PEHA solutions (50 wt% and 75 wt%), a CO_2 capture approach based on Mikkola *et al.*'s work[39] was used, due to the highly viscous nature of these solutions. A continuous CO_2 flow was bubbled with immersed needles into the solutions at 40 °C for 4.5 hours with stirring. The CO_2 capture solutions were then quantitatively analyzed by ^{13}C NMR. The results are shown in Table 1. Generally, as the wt% of PEHA increased, the ratio of carbamate to bicarbonate increased but with a decreased overall CO_2 capacity, in agreement with a literature report.[39] The 11 wt% and 20 wt% solutions differ somewhat, perhaps resulting from the fact that CO_2 not only reacts with PEHA but also dissolves in water. The high viscosity of the concentrated PEHA solutions could also contribute to the lesser capture of CO_2 in these cases.

The subsequent hydrogenation shows a similar trend (Table 1). Generally, as the wt% of PEHA in the starting material increases, the hydrogenated products result in a higher percentage of formamide, with the overall conversion sharply decreases. A high wt% PEHA is unfavorable for the CO_2 conversion. This may arise for two reasons: (a) a high PEHA wt% results in a more viscous CO_2 capture solution, which is likely to limit the diffusion of H_2. (b) A high PEHA wt% results in more unreacted PEHA in the CO_2 capture solution. The presence of a large quantity of unreacted $-NH_2$ groups could potentially poison the AuNP catalyst surface. As a

Table 1 Effect of PEHA wt% on the CO_2 capture species and the hydrogenated products

		CO_2 capture		Hydrogenation[b] Product distribution			
Entry	wt% of PEHA in water	Mole ratio of carbamate : bicarbonate[a]	CO_2 capacity[a] (mmol of CO_2/(g of PEHA))	Formate[c] (%)	Formamide[c] (%)	MeOH[c] (%)	Conversion[c] (%)
1	3.2	1 : 1	14.45	55	44	1	68
2	11	7 : 1	12.73	40	60	0	25
3	20	3 : 1	17.31	18	82	0	3
4	50	16 : 1	8.540	24	76	0	2
5	75	Only carbamate detected	2.518	29	71	0	9

[a] The CO_2 capacity, identification and quantification of carbamate and bicarbonate were determined by quantitative ^{13}C NMR with imidazole as an internal standard. [b] Hydrogenation reaction conditions: 600 μL CO_2 capture solution, 1 mL H_2O containing 5.29 mg Au/SiO_2 and boric acid (1 mol% corresponding to the amount of PEHA presented in the CO_2 capture solution), and 16 bar H_2 (25 °C). The entire system was stirred at 500 rpm, 100 °C for 36 hours. [c] The selectivity and overall conversion were based on ^1H NMR with imidazole as an internal standard.

result, 3.2 wt% PEHA solution was selected for use in subsequent studies.

Screening of reaction conditions

The effect of boric acid. The effect of boric acid on the hydrogenation was investigated (entries 1–4 in Table 2). Compared to boric acid-free conditions, the addition of 1 mol% boric acid significantly improves the overall conversion from 19% to 68%. The addition of 1 mol% boric acid also influences the distribution of three hydrogenated C1 products. Further increasing the boric acid concentration does not change the product distribution significantly but leads to variance in the overall conversion efficiencies.

Additional tests were performed to clarify the role of boric acid. Control experiments are shown in Table 3. When neither boric acid nor Au/SiO_2 is present, the reaction shows a low degree of conversion (10%). It is interesting to note at high temperature and pressure (as per this experiment), the reduction of bicarbonate species to formate will be favorable.[12,40–42] Moreover, the non-catalytic transformation of formate and bicarbonate on exposure to H_2 is known.[43] Thus, a minimal conversion with these conditions is expected (entry 4). With only boric acid but no catalyst (entry 3), the conversion and product distribution were almost identical to entry 4. The promotion effect of boric acid is observed only when Au/SiO_2 also presents (Table 3, entry 1), suggesting that Au/SiO_2 is essential for the observed hydrogenation process.

The pH of the starting material mixture in entry 1, Table 3 is unchanged (7.88 ± 0.05) upon the addition of boric acid. After hydrogenation, the pH of reaction increases to 8.80, likely due to the regeneration of PEHA. Thus, the boric acid most likely serves as a Lewis acid co-catalyst rather than as a pH moderator. Boric acid forms boron esters with carboxylic acid and activates the carboxylic acid. It also forms adducts with amines and carbon dioxide in water.[44–46] In this case, boric acid possibly reduces the energy barrier of the conversion of formic acid (or formate) to formamide (or methanol). On the other hand, boric acid possibly interacts with the carbonate of the reactants, as well as the amine groups of reactants and regenerated PEHA. The reaction yield varies non-systematically with the boric acid concentration, suggesting that a combination of effects of boric acid on the starting materials and intermediates is in play. Moreover, the promoting effect of boric acid only occurred when Au/SiO_2 was present, as shown in Table 3. A recent study[47] involving CO_2 hydrogenation reac-

Table 2 Effect of various experimental parameters on the generation of hydrogenated products

Entry	Mol% of boric acid[a]	Temperature (°C)	H_2 pressure (bar)	Time (h)	Product distribution			Conversion[b] (%)
					Formate[b] (%)	Formamide[b] (%)	MeOH[b] (%)	
1	0	100	16	36	100	0	0	19
2	1	100	16	36	55	44	1	68
3	5	100	16	36	59	41	Trace	8
4	10	100	16	36	41	47	12	15
5	1	120	16	36	53	44	3	66
6	1	80	16	36	54	46	0	26
7	1	100	5	36	34	56	9	12
8	1	100	10	36	55	45	0	11
9	1	100	20	36	40	55	5	37
10	1	100	16	24	49	51	Trace	8
11	1	100	16	48	50	34	16	80

Reaction conditions: 600 μL 3.2 wt% PEHA CO_2 capture solution, 1 mL H_2O containing 5.29 mg Au/SiO_2 and boric acid, and H_2 (25 °C). The entire system was stirred at 500 rpm. [a] Compared to the moles of PEHA presented in the CO_2 capture solution added. [b] The selectivity and overall conversion were based on ^1H NMR with imidazole as an internal standard.

Table 3 Control experiments

Entry	Boric acid	Catalyst	Product distribution			Conversion (%)
			Formate (%)	Formamide (%)	MeOH (%)	
1	+	+	55	44	1	68
2	—	+	100	0	0	19
3	+	—	100	0	0	11
4	—	—	100	0	0	10

"+" means 5.29 mg Au/SiO_2 or 1 mol% boric acid, "—" means none. Reaction conditions: 600 μL CO_2 capture solution, 1 mL H_2O without/with Au/SiO_2 and/or boric acid, and 16 bar H_2 (25 °C). The entire system was stirred at 500 rpm, 100 °C for 36 hours. The selectivity and overall conversion were based on ^1H NMR with imidazole as an internal standard.

tion using SiO_2-supported CuNPs demonstrated that the Lewis acid stabilized formate and methoxy intermediates at the metal surface, resulting in improved MeOH yields and overall conversions. Meanwhile, the activation of CO_2 by the Lewis acid did not require the presence of a metal catalyst surface. Although doping the catalyst with a Lewis acid is not the same as introducing boric acid into the solution, previous research[48] shows that the addition of boric acid to the reactants had similar promotional effects as does doping catalysts. However, the mechanism remained unclear.

The effect of temperature, H_2 pressure, and reaction time. The effect of temperature is reported in Table 2, entries 2, 5, and 6. 100 °C was determined to be the optimal temperature as it was the lowest temperature necessary to ensure a sufficiently high reaction yield (68%).

As the H_2 pressure increases to 16 bar (Table 2, entries 2, 7, 8, and 9), the overall extent of conversion increases. However, when the pressure is increased from 16 bar to 20 bar (Table 2, entries 2 and 9), a decrease in the overall conversion is observed. Although the solubility of H_2 in water increases with H_2 pressure at elevated temperatures,[49] the nucleation of bubbles under the high reaction temperature of 100 °C may inhibit the diffusion of H_2 to the surface of the Au(0) catalyst.[50] Moreover, the porous nature of the catalysts may also promote the formation of bubbles.[51] Both factors complicate the relationship of H_2 pressure and the concentration of soluble H_2 in the aqueous solution.

Finally, the effect of reaction time was investigated (Table 2, entries 2, 10, and 11). Under prolonged reaction times (from 24 hours to 48 hours), the product distribution was little effected whereas the extent of conversion increased. Consideration of all the foregoing observations led to the use of the conditions in Table 2, entry 11.

Recycling test

Results of a reusability test of Au/SiO_2 are shown in Fig. 3. After four cycles of the amine-assisted CO_2 hydrogenation reaction, the yield stabilizes at around 80% of the original yield.

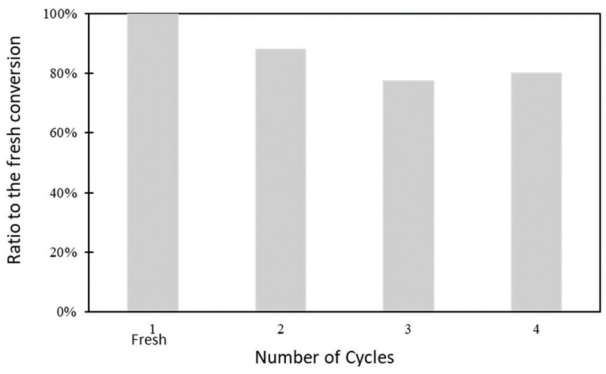

Fig. 3 Reusability test of Au/SiO_2. Reaction conditions: 600 μL 3.2 wt% PEHA CO_2 capture solution, 1 mL H_2O containing 5.29 mg Au/SiO_2 and boric acid (1 mol% corresponding to the amount of PEHA), and 16 bar H_2 (25 °C). The system was stirred at 500 rpm, 100 °C for 48 hours.

The catalyst thus could be used at least four times, equivalent to hydrogenation of CO_2 for a total of eight days. Since the catalyst forms a suspension in water, after each run of the reaction the Au/SiO_2 remains at the bottom of the reaction vessel after settling. No removal of the catalyst was required, the reaction solution was renewed by pipette and a starting material could be added.

Direct reduction of CO_2 presented in the air

CO_2 hydrogenation processes often use pure, pressured CO_2 as the CO_2 source. To demonstrate the capability of this catalytic process in a more "real life" situation, air was used as the CO_2 source. The CO_2 concentration in air at 1 atm is around 400 ppm. Similar to the process demonstrated by Prakash and coworkers,[52] air was bubbled continuously into a 3.2 wt% PEHA solution for 48 hours at room temperature with stirring. The resulted solution was analyzed by quantitative ^{13}C NMR. Compared to CO_2 capture solutions prepared from a high-pressure pure CO_2 source (Table 4, entry 1), the direct CO_2 capture from air (Table 4, entry 2) results in a lower degree of CO_2 absorption and a lower ratio of bicarbonates to carbamates. The subsequent hydrogenation in air has a slightly different distribution of the three products, as well as a lower (but still relatively high) overall conversion (24% compared to 80%). The lower conversion in the air case was probably due to the lower concentration of bicarbonates and carbamates in the starting material, as well as the greater quantity of unreacted PEHA which may serve as a catalyst inhibitor. The former would reduce the reaction rate while the latter would, if active, deactivate the Au surface in the catalyst. The changed product distribution likely results from the effect of different pH values on the reversible hydrolysis/de-hydrolysis process between the formate and formamide. This is discussed in detail in the following mechanistic studies.

Mechanistic studies

Mechanisms associated with the amine-assisted CO_2 hydrogenation catalyzed by ruthenium complexes have been proposed[53,54] to involve a single-channel multi-step process. Species from the previous CO_2 capture step are reduced to formate, which then proceed through a condensation step, producing formamide. Formamide is further reduced to methanol and the original amine. Alternatively, methanol can be generated *via* the direct reduction of formate species.[55,56] While these reactions provide guides to mechanistic discussions, it is necessary to investigate the mechanism of amine-assisted CO_2 hydrogenation catalyzed by the heterogenous Au/SiO_2 catalyst reported here (Table 5).

The origin of formate, formamide, and methanol was examined using two model compounds (ammonium bicarbonate and ammonium carbamate). These two species represent the anticipated PEHA-bicarbonates and PEHA-carbamates respectively. The starting concentrations of ammonium bicarbonate and ammonium carbamate (Table 5, entries 2 and 3) were maintained at the same concentrations of original PEHA-bicarbonates and PEHA-carbamates (Table 5, entry 1), in addition

Table 4 Direct hydrogenation of CO_2 in air

		CO_2 capture				Hydrogenation[b]			
						Production distribution			
Entry	CO_2 source	Contact time (h)	Operation temperature (°C)	Mole ratio of carbamate : bicarbonate[a]	CO_2 capacity[a] (mmol of CO_2/(g of PEHA))	Formate[c] (%)	Formamide[c] (%)	MeOH[c] (%)	Conversion[c] (%)
1	Pure CO_2 (3 bar)	4	70	1 : 1	14.45	50	34	16	80
2	Air (atmospheric pressure)	48	R.T.	5 : 1	8.094	41	34	25	24

[a] The CO_2 capacity, identification and quantification of carbamate and bicarbonate were determined by quantitative ^{13}C NMR with imidazole as an internal standard. [b] Hydrogenation reaction conditions: 600 μL 3.2 wt% PEHA CO_2 capture solution, 1 mL H_2O containing 5.29 mg Au/SiO_2 and boric acid (1 mol% corresponding to the amount of PEHA), and 16 bar H_2 (25 °C). The entire system was stirred at 500 rpm, 100 °C for 48 hours. [c] The selectivity and overall conversion were based on ^1H NMR with imidazole as an internal standard.

to the same additives being present as well as the experimental conditions as entry 1. From the results of entries 2 and 3, ammonium bicarbonate and carbamate were both identified as the source of formate and methanol. The observations here are similar, but not identical to other processes catalyzed by heterogeneous catalysts,[3,57] suggesting that the variety and distribution of hydrogenated products largely depend on the nature of the specific catalyst. The reason why formamide species are not observed in entries 2 and 3 was likely because the low overall conversion made the observation and identification of minor products difficult in the associated ^1H NMR spectra. Thus, from the results associated with bicarbonate and carbamate model compounds, it is proposed that PEHA-bicarbonates and PEHA-carbamates are the source of the three final hydrogenated products (as shown in the first arrow of Scheme 3C).

Additional experiments (ESI, Fig. S18 and S19†) further suggest that methanol is produced after the formation of formate and formamide (Scheme 3C). Studies involving different Au loadings (Fig. S18†) show that the overall conversion and MeOH percentage increased as additional catalyst was added. An increasing quantity of catalyst has a very similar effect on the product distribution as an increased reaction time (Fig. S19†), where all three products increased in quantities with time, although at different rates, causing the product distribution to change with time. Both studies agreed with the mechanism proposed here, where MeOH was formed after formate and formamide. MeOH would thus increase in percentage when given more available active sites or a longer reaction time.

The absence of formamide in Table 5, entries 2 and 3 suggests that methanol directly originates from formate without going through the formamide intermediate (Scheme 3C, Pathway II). To validate the relative likelihood of possible pathways, two compounds, ammonium formate and formamide, were used to as models of PEHA-formate and formamide (Table 5, entries 4 and 5). Reversible conversion between ammonium formate and formamide was observed in both cases, a process known in many classic reactions such as the Leuckart reaction.[58] Specifically, formamide has a higher preference for converting to ammonium formate here, due to the aqueous environment. The conversion between formate and formamide makes it challenging to distinguish Pathway I and Pathway II. Nevertheless, even though the overall conversion yield of ammonium formate hydrogenation is lower compared to the formamide hydrogenation, the ammonium formate example produces a greater relative quantity of methanol. This suggests that Pathway II is the more favorable pathway in terms of methanol formation.

The possibility that only one species is the precursor of methanol arises from consideration of a reversible inter-conversion between formate and formamide. To further validate Pathways I and II, formamide hydrogenation was conducted in ^{18}O-labeled water. If formamide is the principal precursor of methanol, the resulting methanol would be predominately $Me^{16}OH$. On the other hand, if formate is the principal precur-

Table 5 Mechanistic studies of amine-assisted CO_2 hydrogenation catalyzed by Au/SiO_2

		Production distribution			
Entry	Carbon source	Formate (%)	Formamide (%)	MeOH (%)	Conversion (%)
1	CO_2 captured 3.2 wt% PEHA	55	44	1	68
2	Ammonium bicarbonate	19	0	81	17
3	Ammonium carbamate	22	0	78	11
4	Formamide	20	79	1	21
5	Ammonium formamide	95	2	3	5

Reaction conditions: 600 μL CO_2 capture solution or corresponding solution, 1 mL H_2O with 5.294 mg Au/SiO_2 and 1 mol% boric acid, and 16 bar H_2 (25 °C). The entire system was stirred at 500 rpm, 100 °C for 36 hours. The starting concentrations of ammonium bicarbonate and ammonium carbamate (entries 2 and 3) were kept the same as the concentrations of original PEHA-bicarbonates and PEHA-carbamates (entry 1). The starting concentration of formamide and ammonium formate (entries 4 and 5) were kept the same as the concentrations of formamide and formate (entry 1).

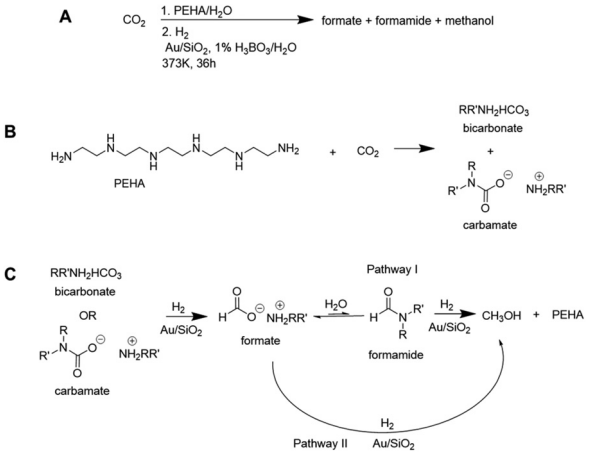

Scheme 3 Reaction schemes associated with the experimental procedures and observations. (A) The overall reaction. (B) The CO_2 capture process by PEHA. (C) The hydrogenation process in the presence of the Au/SiO_2 catalyst, highlighting two proposed pathways leading to CH_3OH.

sor, ^{18}O- and ^{16}O-methanol would be observed in a 1 : 1 ratio. The isotopic experiment was run under conditions identical to Table 5, entry 4, except that water was replaced with $H_2{}^{18}O$. GC-MS analysis of the hydrogenation products (ESI, Fig. S15B†) demonstrates the presence of both $Me^{18}OH$ and $Me^{16}OH$, with $Me^{18}OH$ being predominant. To quantify the ratio of $Me^{18}OH$ to $Me^{16}OH$, the quantity of $Me^{16}OH$ based on a calibration curve of ion fragment abundances of m/z = 29 ($CH^{16}O^+$) *vs.* $Me^{16}OH$ concentration was determined. Using the total amount of methanol determined by ^1H NMR with an internal standard, a mole ratio of $Me^{18}OH$ to $Me^{16}OH$ of 3.5 : 1 is observed (details in ESI†). Several factors may lead to a $Me^{18}OH$ to $Me^{16}OH$ ratio that is greater than 1 : 1. Firstly, oxygen isotope effects may influence the hydrolysis of formamide[59] as well as the hydrogenation of formate and formamide. Secondly, the higher ^{18}O percentage in the final methanol could arise from further exchange of ^{16}O by ^{18}O-water in formate.[60] Thirdly, heterogenous catalysts including supported gold nanoparticles have been reported to contribute to significant kinetic isotopic effects in exchange, chemisorption and hydrogenation in terms of deuterium and hydrogen.[61,62] Finally, the condensation of ammonium formate to formamide, although unfavourable, could still be possible and needs to be taken into account (ESI, Fig. S17†). As entries 4 and 5 in Table 5 demonstrate, formate and formamide are convertible although the model compounds differ from the real PEHA-involved situation. Taking all these observations into consideration, a mechanism for CO_2 hydrogenation to methanol is proposed to involve Pathway II, and formate as the primary precursor.

It is important to note that the product distributions, as well as the overall conversions in model compound studies, differ from those in the actual PEHA-CO_2-H_2 experiment (Table 5, entry 1). A small cation like NH_4^+ is significantly different than the protonated PEHA in terms of both its size/volume and hydrophobicity. Moreover, the pH of the two solutions differs during reaction. The amine-assisted CO_2 hydrogenation process exhibits pH changes during the reaction (see section Screening of reaction conditions), suggesting that pH plays a role in the equilibrium between formate species and formamide species. The pH in turn influences the distribution between Pathway I and Pathway II, and finally impacts the product distribution and overall conversion. A reaction mechanism consistent with these results is presented in Scheme 3.

Conclusions

A novel mesoporous-silica-supported Au(0) nanoparticle catalyst combined with amines leads to the conversion of CO_2 to formate, formamide, and methanol without the use of organic solvent. The conversion reaches 80% at 100 °C and 16 bar H_2 over 48 hours. The Au(0) catalyst is mechanically stable, well-nanostructured, and readily reusable for multiple runs without separation procedures. Detailed mechanistic studies clarify the carbon conversion process where both CO_2 capture species (bicarbonate and carbamate) are the source of the three reduced products. The methanol product originates from two pathways – direct hydrogenation from formate and

indirect hydrogenation involving formamide intermediates. Semiquantitative isotope labelling studies suggest that formate is the principal precursor of the methanol product. Most importantly, this facile one-pot Au/SiO_2 catalyst system is capable of using ambient air as a CO_2 source. It also exhibits the capability of catalytically producing methanol and formate from carbon sources such as inorganic bicarbonate and carbamate salts. These findings demonstrate the versatility of the Au/SiO_2 catalyst in green chemistry applications, especially in the conversion of CO_2 directly from air when coupled with advanced direct air capture (DAC) techniques in the future.

Funding

This work was supported by Natural Sciences and Engineering Research Council (NSERC) and by Fonds Québécois de la Recherche sur la Nature et les Technologies (FQRNT).

Conflicts of interest

The authors declare that they have no competing interests.

Acknowledgements

The authors would like to thank Dr Xue-Dong Liu (FEMR, McGill) for the TEM imaging, Dr Robin Stein (McGill Chemistry Characterization Facility) and Dr Tara Sprules (Quebec/Eastern Canada High Field NMR Facility) for assistance in quantitative ^{13}C NMR. S. N. would like to thank Sosthène Ung (C-J Li Lab, Deparment of Chemistry, McGill) for assistance in GC-MS methodology development in the ^{18}O isotopic study.

References

1 National Oceanic and Atmospheric Administration, Earth System Research Laboratory, Global Monitoring Division, *Global Greenhouse Gas Reference Network-Trends in Atmospheric Carbon Dioxide*, U.S. Department of Commerce, Mauna Loa, Hawaii, U.S., February 5, 2020.
2 X. Jiang, X. Nie, X. Guo, C. Song and J. G. Chen, *Chem. Rev.*, 2020, **120**(15), 7984–8034.
3 T. Wang, D. Ren, Z. Huo, Z. Song, F. Jin, M. Chen and L. Chen, *Green Chem.*, 2017, **19**, 716–721.
4 X.-L. Du, Z. Jiang, D. S. Su and J.-Q. Wang, *ChemSusChem*, 2016, **9**, 322–332.
5 W.-H. Wang, Y. Himeda, J. T. Muckerman, G. F. Manbeck and E. Fujita, *Chem. Rev.*, 2015, **115**, 12936–12973.
6 E. S. Sanz-Pérez, C. R. Murdock, S. A. Didas and C. W. Jones, *Chem. Rev.*, 2016, **116**, 11840–11876.
7 S. Kar, R. Sen, A. Goeppert and G. K. S. Prakash, *J. Am. Chem. Soc.*, 2018, **140**, 1580–1583.
8 A. Galadima and O. Muraza, *Renewable Sustainable Energy Rev.*, 2019, **115**, 109333.
9 D. A. Bulushev and J. R. H. Ross, *Catal. Rev.*, 2018, **60**, 566–593.
10 S. Kar, A. Goeppert and G. K. S. Prakash, *Acc. Chem. Res.*, 2019, **52**, 2892–2903.
11 L. Álvarez de Cienfuegos, R. Robles, D. Miguel, J. Justicia and J. M. Cuerva, *ChemSusChem*, 2011, **4**, 1035–1048.
12 S. Moret, P. J. Dyson and G. Laurenczy, *Nat. Commun.*, 2014, **5**, 4017.
13 A. Bosoaga, O. Masek and J. E. Oakey, *Energy Procedia*, 2009, **1**, 133–140.
14 A. J. Hunt, E. H. K. Sin, R. Marriott and J. H. Clark, *ChemSusChem*, 2010, **3**, 306–322.
15 H. Zhong, M. Iguchi, M. Chatterjee, T. Ishizaka, M. Kitta, Q. Xu and H. Kawanami, *ACS Catal.*, 2018, **8**, 5355–5362.
16 S. Masuda, K. Mori, Y. Futamura and H. Yamashita, *ACS Catal.*, 2018, **8**, 2277–2285.
17 K. Mori, T. Sano, H. Kobayashi and H. Yamashita, *J. Am. Chem. Soc.*, 2018, **140**, 8902–8909.
18 P. Patel, S. Nandi, M. S. Maru, R. I. Kureshy and N.-u. H. Khan, *J. CO2 Util.*, 2018, **25**, 310–314.
19 H. Sakurai and M. Haruta, *Appl. Catal., A*, 1995, **127**, 93–105.
20 H. Sakurai, S. Tsubota and M. Haruta, *Appl. Catal., A*, 1993, **102**, 125–136.
21 C. Wu, P. Zhang, Z. Zhang, L. Zhang, G. Yang and B. Han, *ChemCatChem*, 2017, **9**, 3691–3696.
22 D. Preti, C. Resta, S. Squarcialupi and G. Fachinetti, *Angew. Chem., Int. Ed.*, 2011, **50**, 12551–12554.
23 G. A. Filonenko, W. L. Vrijburg, E. J. M. Hensen and E. A. Pidko, *J. Catal.*, 2016, **343**, 97–105.
24 C. Wu, Z. Zhang, Q. Zhu, H. Han, Y. Yang and B. Han, *Green Chem.*, 2015, **17**, 1467–1472.
25 Q. Liu, X. Yang, L. Li, S. Miao, Y. Li, Y. Li, X. Wang, Y. Huang and T. Zhang, *Nat. Commun.*, 2017, **8**, 1407.
26 S. K. Beaumont, S. Alayoglu, C. Specht, N. Kruse and G. A. Somorjai, *Nano Lett.*, 2014, **14**, 4792–4796.
27 S. Kiatphuengporn, M. Chareonpanich and J. Limtrakul, *Chem. Eng. J.*, 2014, **240**, 527–533.
28 E. M. Fiordaliso, I. Sharafutdinov, H. W. P. Carvalho, J.-D. Grunwaldt, T. W. Hansen, I. Chorkendorff, J. B. Wagner and C. D. Damsgaard, *ACS Catal.*, 2015, **5**, 5827–5836.
29 N. Koizumi, X. Jiang, J. Kugai and C. Song, *Catal. Today*, 2012, **194**, 16–24.
30 A. S. Alshammari, *Catalysts*, 2019, **9**, 402.
31 H.-K. Na, M.-H. Kim, K. Park, S.-R. Ryoo, K. E. Lee, H. Jeon, R. Ryoo, C. Hyeon and D.-H. Min, *Small*, 2012, **8**, 1752–1761.
32 M. Mizutani, Y. Yamada, T. Nakamura and K. Yano, *Chem. Mater.*, 2008, **20**, 4777–4782.
33 V. J. Gandubert and R. B. Lennox, *Langmuir*, 2005, **21**, 6532–6539.
34 L. Gomez, V. Sebastian, M. Arruebo, J. Santamaria and S. B. Cronin, *Phys. Chem. Chem. Phys.*, 2014, **16**, 15111–15116.

35 S. Schünemann, G. Dodekatos and H. Tüysüz, *Chem. Mater.*, 2015, **27**, 7743–7750.
36 L.-F. Gutiérrez, S. Hamoudi and K. Belkacemi, *Catalysts*, 2011, **1**, 97–154.
37 S. Arrii, F. Morfin, A. J. Renouprez and J. L. Rousset, *J. Am. Chem. Soc.*, 2004, **126**, 1199–1205.
38 M. Sivakumar, K. Venkatakrishnan and B. Tan, *Nanoscale Res. Lett.*, 2011, **6**, 78.
39 T. Q. Bui, S. G. Khokarale, S. K. Shukla and J.-P. Mikkola, *ACS Sustainable Chem. Eng.*, 2018, **6**, 10395–10407.
40 J. M. Heltzel, M. Finn, D. Ainembabazi, K. Wang and A. M. Voutchkova-Kostal, *Chem. Commun.*, 2018, **54**, 6184–6187.
41 H. Wiener, J. Blum, H. Feilchenfeld, Y. Sasson and N. Zalmanov, *J. Catal.*, 1988, **110**, 184–190.
42 G. Laurenczy, F. Joó and L. Nádasdi, *Inorg. Chem.*, 2000, **39**, 5083–5088.
43 S. Chao, C. J. Stalder, D. P. Summers and M. S. Wrighton, *J. Am. Chem. Soc.*, 1984, **106**, 2723–2725.
44 K. Hakan, *Bor Dergisi*, 2018, **3**, 1–7.
45 R. Pal, *ARKIVOC*, 2018, **1**, 346–371.
46 B. D. Vineyard and H. C. Godt, *Inorg. Chem.*, 1964, **3**, 1144–1147.
47 C. Copéret, G. Noh, E. Lam, D. T. Bregante, J. Meyet, P. Šot and D. W. Flaherty, *Angew. Chem., Int. Ed.*, 2021, **60**, 9650–9659.
48 S. U. Nandanwar, A. A. Dabbawala, M. Chakraborty, H. C. Bajaj, S. Mukhopadhyay and K. T. Shenoy, *Res. Chem. Intermed.*, 2016, **42**, 1557–1569.
49 V. I. Baranenko and V. S. Kirov, *Sov. Atom. Energ.*, 1989, **66**, 30–34.
50 S. D. Lubetkin, *Langmuir*, 2003, **19**, 2575–2587.
51 C. Y. Lee, M. M. H. Bhuiya and K. J. Kim, *Int. J. Heat Mass Transfer*, 2010, **53**, 4274–4279.
52 J. Kothandaraman, A. Goeppert, M. Czaun, G. A. Olah and G. K. S. Prakash, *J. Am. Chem. Soc.*, 2016, **138**, 778–781.
53 S. Kar, R. Sen, J. Kothandaraman, A. Goeppert, R. Chowdhury, S. B. Munoz, R. Haiges and G. K. S. Prakash, *J. Am. Chem. Soc.*, 2019, **141**, 3160–3170.
54 N. M. Rezayee, C. A. Huff and M. S. Sanford, *J. Am. Chem. Soc.*, 2015, **137**, 1028–1031.
55 E. Balaraman, C. Gunanathan, J. Zhang, L. J. W. Shimon and D. Milstein, *Nat. Chem.*, 2011, **3**, 609–614.
56 A. Tsurusaki, K. Murata, N. Onishi, K. Sordakis, G. Laurenczy and Y. Himeda, *ACS Catal.*, 2017, **7**, 1123–1131.
57 J. Su, M. Lu and H. Lin, *Green Chem.*, 2015, **17**, 2769–2773.
58 C. Pollard and D. C. Young, *J. Org. Chem.*, 1951, **16**, 661–672.
59 J. F. Marlier, N. C. Dopke, K. R. Johnstone and T. J. Wirdzig, *J. Am. Chem. Soc.*, 1999, **121**, 4356–4363.
60 M. A. Rishavy and W. W. Cleland, *Can. J. Chem.*, 1999, **77**, 967–977.
61 S. Naito and M. Tanimoto, *J. Chem. Soc., Chem. Commun.*, 1988, **12**, 832–833.
62 C. Mirodatos, *Catal. Today*, 1991, **9**, 83–95.